Mechanisms of Southern Ocean Heat Uptake and Transport in a Global Eddying Climate Model

ADELE K. MORRISON

Princeton University, Princeton, New Jersey

STEPHEN M. GRIFFIES, MICHAEL WINTON, AND WHIT G. ANDERSON

NOAA/Geophysical Fluid Dynamics Laboratory, Princeton, New Jersey

JORGE L. SARMIENTO

Princeton University, Princeton, New Jersey

(Manuscript received 15 August 2015, in final form 25 November 2015)

ABSTRACT

The Southern Ocean plays a dominant role in anthropogenic oceanic heat uptake. Strong northward transport of the heat content anomaly limits warming of the sea surface temperature in the uptake region and allows the heat uptake to be sustained. Using an eddy-rich global climate model, the processes controlling the northward transport and convergence of the heat anomaly in the midlatitude Southern Ocean are investigated in an idealized 1% yr^{-1} increasing CO_2 simulation. Heat budget analyses reveal that different processes dominate to the north and south of the main convergence region. The heat transport northward from the uptake region in the south is driven primarily by passive advection of the heat content anomaly by the existing time mean circulation, with a smaller 20% contribution from enhanced upwelling. The heat anomaly converges in the midlatitude deep mixed layers because there is not a corresponding increase in the mean heat transport out of the deep mixed layers northward into the mode waters. To the north of the deep mixed layers, eddy processes drive the warming and account for nearly 80% of the northward heat transport anomaly. The eddy transport mechanism results from a reduction in both the diffusive and advective southward eddy heat transports, driven by decreasing isopycnal slopes and decreasing along-isopycnal temperature gradients on the northern edge of the peak warming.

1. Introduction

Over recent decades, the ocean has absorbed 93% of the additional energy in the climate system arising from global warming (Levitus et al. 2012). Subsurface ocean heat gain has had a beneficial impact thus far through limiting atmospheric warming. However, ocean heat gain also leads to increasingly significant sea level rise, slower ocean carbon uptake, and potentially accelerated melting of the Antarctic ice sheets (IPCC 2013). The Southern Ocean has been recognized as an important region for ocean heat uptake, dominating the net global uptake (Durack et al. 2014; Frölicher et al. 2015; Roemmich et al. 2015).

In situ temperature measurements reveal that the subsurface Southern Ocean has warmed at a faster rate than the global average over recent decades. Decadal warming trends are maximum between 40° and 55°S and extend deeper than 1000 m at rates of 0.1°–0.2°C $decade^{-1}$ (e.g., Gille 2002; Böning et al. 2008). Durack et al. (2014) suggest that these trend estimates may even be biased low, because of limitations of the analysis methods used in data-sparse regions. Roemmich et al. (2015) show that, over the shorter period 2006–13, which has extensive Argo float coverage, 67%–98% of the global upper ocean (0–2 km) heat content anomaly is accounted for by the Southern Ocean (20°–60°S), with a significant peak around 40°–45°S.

Corresponding author address: Adele K. Morrison, Program in Atmospheric and Oceanic Sciences, Princeton University, 300 Forrestal Rd., Princeton, NJ 08544.
E-mail: adelem@princeton.edu

DOI: 10.1175/JCLI-D-15-0579.1

© 2016 American Meteorological Society

Unauthenticated | Downloaded 04/30/25 11:23 AM UTC

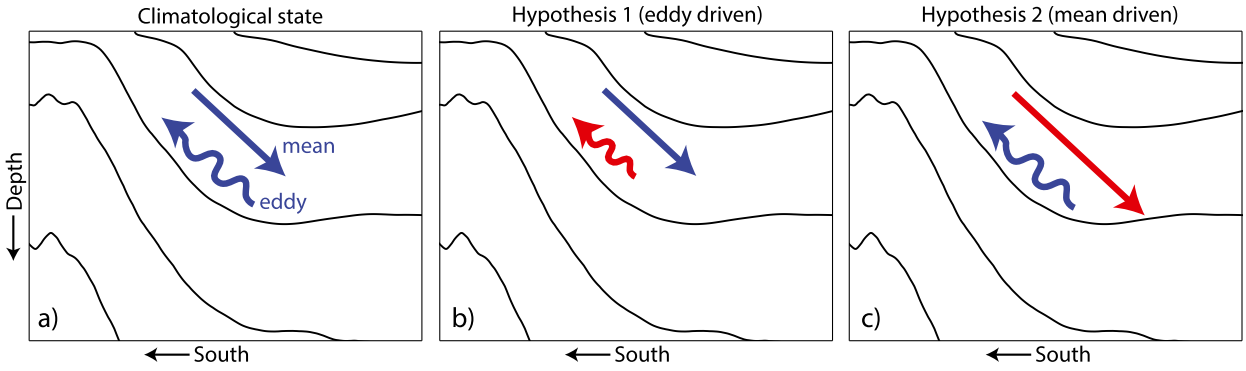

FIG. 1. Schematic showing the two hypotheses for how a heat anomaly may be transported into the Southern Ocean interior. (a) In the climatological state, the mean and eddy heat transport (arrows) are approximately balanced. (b) Hypothesis 1: the upward/southward eddy heat transport decreases. (c) Hypothesis 2: the downward/northward mean heat transport increases. Blue arrows show climatological or unchanged heat fluxes; shorter (longer) red arrows show reduced (increased) heat fluxes.

While intensified heat uptake by the Southern Ocean is also a ubiquitous feature of climate change simulations (e.g., Stouffer et al. 2006; Cai et al. 2010; Kuhlbrodt and Gregory 2012; Frölicher et al. 2015), the magnitude of heat uptake varies enormously between different models. In phase 5 of the Coupled Model Intercomparison Project (CMIP5) model suite, the standard deviation of the multimodel mean heat uptake over the Southern Ocean is ±40% (Frölicher et al. 2015). This is in stark contrast to the modeled CO_2 uptake in the Southern Ocean, for which the CMIP5 standard deviation is only ±10% of the multimodel mean (Frölicher et al. 2015). While Southern Ocean CO_2 uptake, at this stage, appears to be controlled to first order simply by the elevated atmospheric CO_2 concentration, ocean heat uptake is more strongly dependent on a multitude of complex climate processes, including changing ocean circulation, eddies, and vertical diffusion, as well as atmospheric processes such as aerosols and cloud feedbacks. Our aim in this paper is to improve understanding of the role of ocean processes, in particular the mesoscale and overturning circulation, in contributing to the intense Southern Ocean heat uptake and the unique pattern of deep, midlatitude warming.

Drivers of the northward heat transport anomaly

Ocean heat uptake is high in the Southern Ocean because of the large-scale upwelling that exposes colder water masses to the atmosphere (Morrison et al. 2015, and references therein). Strong westerly winds drive an Ekman divergence south of ~50°S at the surface, which draws up deep waters from below. Upon reaching the surface, some of the upwelled waters are driven northward in the Ekman layer, warming and freshening as they travel north. The Ekman divergence continually upwells more cold waters, keeping the sea surface temperature low even as the atmosphere continues to warm, thereby driving additional heat into the ocean under climate change. The Southern Ocean midlatitude warming pattern evident in models and observations reveals that once the heat is absorbed at the surface over the upwelling region (~50°–60°S), it is transported northward and downward (e.g., Marshall et al. 2015; Frölicher et al. 2015). This ocean heat transport anomaly is significant because it assists in keeping sea surface temperatures low, thereby allowing additional heat uptake at the surface.

It remains unclear from previous studies as to whether the heat transport anomaly away from the surface in the Southern Ocean is dominated by mean or eddy contributions. In numerical models, the climatological heat budget in the interior Southern Ocean is a balance between northward/downward heat transport by the time mean advective flow and southward/upward heat transport by eddies (e.g., Gregory 2000; Wolfe et al. 2008). Modeling studies have found that this balance can be modified in two primary ways, both resulting in warming of the subsurface Southern Ocean. As illustrated conceptually in Fig. 1, either the southward/upward eddy heat transport can decrease (Gregory 2000; Dalan et al. 2005; Morrison et al. 2013), or the wind-driven northward/downward advective heat transport can increase (Cai et al. 2010; Marshall and Zanna 2014; Bryan et al. 2014; Exarchou et al. 2015; Kuhlbrodt et al. 2015).

The first, eddy-based mechanism was highlighted by Gregory (2000). Because of the high precipitation over the Southern Ocean, the surface waters are fresher than at depth. Therefore the temperature along an isopycnal increases with depth (i.e., the reverse of the vertical temperature gradient). As a result, eddy stirring on isopycnals (i.e., isopycnal diffusion) gives rise to an along-isopycnal heat transport directed upward and

Unauthenticated | Downloaded 04/30/25 11:23 AM UTC

southward in the climatological state. In climate change scenarios, the surface intensified warming decreases the along-isopycnal temperature gradient, thereby reducing the upward eddy heat flux. Such a reduction in isopycnal diffusion was found to be the dominant driver of mid-depth Southern Ocean warming in the coarse-resolution models used by Gregory (2000) and Dalan et al. (2005) and in the idealized eddy-permitting model of Morrison et al. (2013).

The second mechanism that has been found to drive Southern Ocean warming in models is enhanced heat advection along the pathway of the upper overturning cell (Cai et al. 2010; Marshall and Zanna 2014; Bryan et al. 2014; Exarchou et al. 2015; Kuhlbrodt et al. 2015). In this case, the primary pathway for the heat anomaly to enter the ocean is first northward in the surface Ekman layer, followed by subduction along isopycnals into the mode and intermediate water masses. However, these studies, by construction, may be underestimating the role of isopycnal diffusion: Marshall and Zanna (2014) do not include salinity in their conceptual model (and therefore have no isopycnal temperature gradients), while Exarchou et al. (2015) show that many coarse-resolution models drastically limit parameterized isopycnal diffusion in regions of steep isopycnal slopes (i.e., much of the upper Southern Ocean). It therefore remains unclear as to whether decreasing eddy (isopycnal) heat diffusion or increasing mean heat advection is the dominant mechanism for transporting the heat anomaly into the interior Southern Ocean.

A second open question regards the extent to which changes in the overturning circulation contribute to heat uptake. In models where the second mechanism (mean advection) dominates the northward heat transport anomaly, the heat uptake is sustained primarily by additional heat transported northward and downward via the overturning circulation. The temperature transport anomaly can be written as

$$\Delta(v\theta) = v(\Delta\theta) + (\Delta v)\theta + \Delta v\Delta\theta, \qquad (1)$$

where v is meridional velocity, θ is potential temperature, and Δ indicates the climate change anomaly. There is some disagreement between previous studies (Winton et al. 2013; Marshall et al. 2015; Exarchou et al. 2015) regarding the relative roles of changes in velocity $[(\Delta v)\theta]$ or temperature $[v(\Delta\theta)]$ or both $[\Delta v\Delta\theta]$ in driving the enhanced heat transport. Observations show that Southern Ocean temperatures are increasing, meaning that the enhanced heat transport could be simply passive advection by the existing circulation [i.e., as represented by the term $v(\Delta\theta)$ (e.g., Marshall et al. 2015)]. However, it has been hypothesized that the upwelling and northward surface transport has increased in response to elevated wind stress over recent decades (Waugh et al. 2013). It is possible that enhanced upwelling of cold waters and more rapid northward transport of the heat anomaly has assisted in keeping sea surface temperatures low, thereby leading to increased heat uptake [i.e., as represented by the term $(\Delta v)\theta$].

The many outstanding questions regarding the mechanisms driving deep Southern Ocean warming provide the motivation for this study. In particular, this paper investigates what sets the unique pattern of deep-reaching, midlatitude warming in the Southern Ocean (section 3). Using an eddy-rich global climate model, with explicitly resolved isopycnal diffusion, we are able to quantify the relative roles of changes in the mean and eddy heat transports and convergences (section 4). Through a detailed model heat budget analysis, we also investigate to what extent increased upwelling contributes to the enhanced mean heat advection (section 5).

2. Model configuration and simulations

We use the high-resolution GFDL global climate model CM2.6, which consists of a nominally 0.1° resolution ocean model coupled to an atmospheric model with approximately 50-km resolution, along with sea ice and land models. In this section, we provide details of the configuration of the ocean component, because the study focuses primarily on processes related to ocean heat transport. The other model components are described in further detail in Delworth et al. (2012) and Griffies et al. (2015).

Based on the resolution criteria of Hallberg (2013)—that the grid spacing needs to be less than half of the baroclinic deformation radius—CM2.6 resolves ocean eddies equatorward of ~55°S. To avoid damping eddy activity, a low viscosity with a Smagorinsky biharmonic friction operator is used (Griffies and Hallberg 2000). Figure 1 in Griffies et al. (2015) illustrates that the mesoscale variability in CM2.6 compares well with satellite altimeter analysis from Archiving, Validation, and Interpolation of Satellite Oceanographic Data (AVISO) (Le Traon et al. 1998; Ducet et al. 2000) over the Southern Ocean. As the model resolves eddies over the majority of the global ocean, no parameterizations are employed for either eddy advection or eddy diffusion in CM2.6. Despite the significant improvements in CM2.6 compared with previous lower-resolution models, for example in the ocean temperature bias (Delworth et al. 2012; Griffies et al. 2015), there remain deficiencies in large regions along coastlines, near Antarctica, in the Arctic, and in much of the North Atlantic where the model may not even be considered eddy permitting.

Unauthenticated | Downloaded 04/30/25 11:23 AM UTC

However, over the latitude range where the peak heat content anomaly occurs in the simulation (30°–55°S), the ocean model grid spacing is sufficient to resolve eddies.

The ocean component of CM2.6 uses the MOM5 code (Griffies 2012), with a z^* generalized vertical coordinate. There are 50 vertical levels distributed throughout the ocean column down to 5500 m. When the ocean is at rest, the layer thicknesses vary smoothly from 10 m in the upper ocean to 210 m at the bottom. Resolved ocean tracer advection in CM2.6 is computed using a third-order piecewise parabolic method. To account for the unresolved impact of submesoscale eddies in the ocean mixed layer, the Fox-Kemper et al. (2011) parameterization restratifies near the surface, thereby contributing significantly to tracer transport within the mixed layer. The model has no prescribed background vertical diffusion, but rather a number of specific physical parameterizations for vertical mixing processes, including internal gravity wave breaking, coastal mixing, internal shear mixing, and a KPP surface boundary layer scheme (Large et al. 1994). Regions of gravitational instability are stabilized by enhancing both the vertical diffusivity and viscosity. CM2.6 does not make use of an overflow parameterization and therefore has a weak lower overturning cell [see Fig. 1 in Dufour et al. (2015)].

A preindustrial control simulation of CM2.6 is spun up for 120 years, with atmospheric CO_2 concentration fixed at 286 ppm. The ocean is initialized from observed climatological temperature and salinity fields. An 80-yr idealized climate change simulation, in which atmospheric CO_2 increases at a rate of 1% yr^{-1}, is split off from the preindustrial control after the 120-yr spinup. We refer to the starting year of the climate change experiment as year 1. Atmospheric CO_2 reaches double its initial value at year 70, then continues to increase for a further 10 yr until the end of the climate change simulation. Unless otherwise specified, the results shown are 20-yr averages at the end of the simulation [i.e., centered around the time of CO_2 doubling (years 61–80)], with anomalies calculated relative to the same time period in the preindustrial control simulation. Given the short time scale of the spinup and experiment (200 yr total), the preindustrial control climate is not in equilibrium. However, this approach does have the advantage that the simulation remains relatively close to observations. Griffies et al. (2015) show that, compared with other similar coarse-resolution or eddy-permitting coupled models, CM2.6 also has a relatively small drift away from the initial climatology. A comparison of the fidelity of the simulated Southern Ocean in CM2.6 to observed values may be found in Dufour et al. (2015), including Antarctic Circumpolar Current transport time series, overturning circulation streamfunction, sea surface temperature, and sea surface salinity.

3. Distribution of Southern Ocean heat uptake and storage

We first consider the modeled surface heat flux anomaly (i.e., net heat uptake), integrated over the 80 yr of the idealized 1% yr^{-1} increasing CO_2 simulation (black line, Fig. 2a). The largest zonally integrated heat uptake occurs in the Southern Ocean, between 50° and 60°S. This latitude range aligns with the region where the upwelling waters reach the base of the winter mixed layer (not shown). The heat uptake south of 30°S accounts for 51% of the net global uptake in CM2.6. In the control simulation, the sea surface temperature is on average warmer than the atmosphere over most of the Southern Ocean, and therefore the sensible heat flux cools the ocean. The prominent Southern Ocean heat uptake peak, between 50° and 60°S, is dominated by a positive anomaly (i.e., a reduction in cooling) in the sensible heat flux component (blue line), related to the decreasing air–sea temperature difference. The presence of upwelling deep waters maintains a relatively constant sea surface temperature (SST) in the high-latitude Southern Ocean, and the atmosphere above warms faster than the ocean, thereby reducing the air–sea temperature gap. Figure 2b shows the climate-change-induced anomaly in the temperature difference between either the overlying atmosphere or sea ice (taken as the ocean freezing point temperature) and the ocean surface. Red shading indicates the spatial pattern of where a positive sensible heat flux anomaly may be expected from the temperature difference anomaly, which is in agreement with the zonally integrated sensible heat flux in Fig. 2a (blue line). To the north of the climatological winter sea ice extent (solid black line in Fig. 2b) there is a large change in the atmosphere–ocean temperature difference as a result of the rapidly warming atmosphere and slowly warming sea surface at these latitudes. To the south of the climatological winter sea ice extent, the change in the atmosphere/sea ice–ocean temperature difference indicates more cooling from the sensible heat flux, compared with the control simulation. This is a result of retreating sea ice, such that regions covered by sea ice in the control experiment are more frequently exposed to the much colder atmosphere in the climate change experiment. The intense dipole pattern in the Weddell Sea is caused by a zonal shift of the open polynya between the control and climate change experiments, but this has only a minor impact on the zonally integrated heat flux (see blue line in Fig. 2a). A reduction in the sensible heat flux also dominates the Southern Ocean heat uptake in the CMIP5 simulations (Frölicher et al. 2015). South of

Unauthenticated | Downloaded 04/30/25 11:23 AM UTC

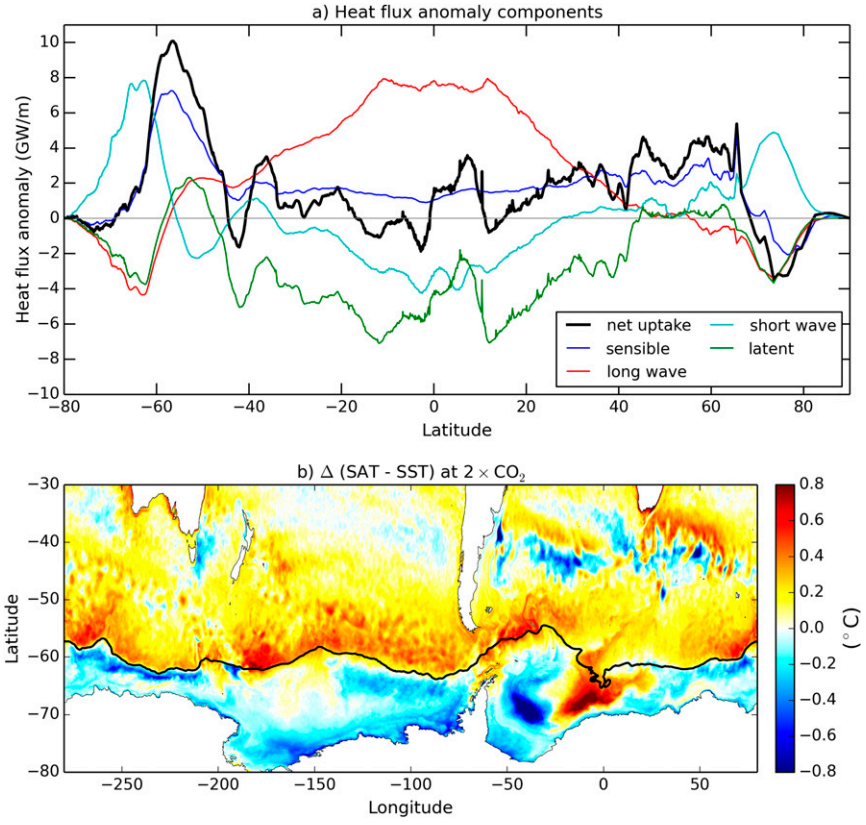

FIG. 2. (a) Change in air–sea heat flux components, with the net air–sea heat flux anomaly in black, for the 1% yr^{-1} CO_2 simulation relative to the control, integrated over years 1–80. Colors show heat flux components, as indicated in the legend. Note that the latent term (green) includes contributions from precipitation, evaporation, ice bergs, frazil sea ice formation, and changes in runoff. (b) The change in air–sea temperature difference in the final 20 yr of the climate experiment relative to the control simulation. The temperature difference is calculated daily, and, in the presence of sea ice, the ocean freezing point temperature is used instead of atmospheric temperature. The thick black line indicates the annual average 0.15 sea ice extent in the control simulation. Red (blue) areas indicate where a positive (negative) anomaly in the sensible heat flux may be expected.

60°S, a decrease in sea ice in the climate change experiment leads to increased exposure of the ocean to the atmosphere. Without the sea ice to insulate the ocean, there is a large increase in shortwave absorption by the ocean, compensated by increased cooling due to evaporation (latent heat flux) and longwave radiation. These sea ice–induced changes south of 60°S nearly exactly cancel one another so that the sensible heat flux dominates the net heat uptake.

The distribution of the additional ocean heat storage in the climate change experiment is shown in Fig. 3. Consistent with the pattern of warming in the CMIP5 historical simulations (Frölicher et al. 2015) and the recent Argo trend (Roemmich et al. 2015), there is a distinct zonal band of ocean heat storage at 40°–45°S, extending to more than 1000-m depth. Notably, the maximum heat storage is located ~10° farther north than the peak heat flux shown in Fig. 2a, implying an increase in the northward and downward transport of heat in the ocean. The storage peak is a persistent feature throughout the duration of the climate change simulation, remaining fixed between 40° and 45°S, rather than progressing northward. The maximum zonal average Southern Ocean temperature trend at 500-m depth, averaged over the full length of the climate change simulation is 0.18°C $decade^{-1}$. Though the simulation is driven by idealized 1% yr^{-1} increasing CO_2 forcing, rather than realistic climate change forcing (including ozone, aerosols, solar changes, etc.), the simulated heat uptake is the same order of magnitude as the current observed estimates of 0.1°–0.2°C $decade^{-1}$ (Gille 2002; Böning et al. 2008).

Figure 4 shows a close-up of the Southern Ocean portion of Fig. 3b and the relationship of the heat

Unauthenticated | Downloaded 04/30/25 11:23 AM UTC

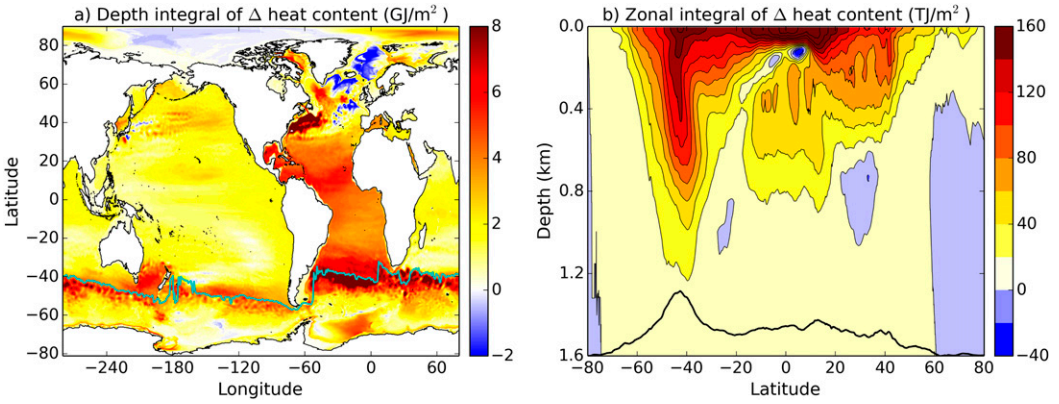

FIG. 3. Spatial distribution of the (a) depth-integrated (10^9 J m^{-2}) and (b) zonally integrated (10^{12} J m^{-2}) ocean heat content anomaly at the time of CO_2 doubling (averaged over years 61–80). The circumpolar cyan line at approximately 40°S in (a) indicates the latitude of the annual maximum mixed layer depth in the Southern Hemisphere midlatitudes. The thick black line in the lower part of (b) shows the full depth and zonal integral of the ocean heat content change, with a range of 0–1.3 × 10^{17} J m^{-1}.

storage pattern to water mass locations. Contours of minimum potential vorticity are shown in gray, indicating Subantarctic Mode Water. Green lines show salinity contours, indicating the freshwater tongue extending down from the surface, aligned with Antarctic Intermediate Water. The maximum warming is positioned between the mode and intermediate waters. Interestingly, there is minimal warming extending northward into the mode waters, despite this being the primary advective pathway into the interior ocean. Instead, the heat content anomaly remains largely to the south of the deep mixed layers in the Southern Ocean (shown by the cyan line at ~40°S in Fig. 3a), which are the formation regions of the mode waters.

In the following two sections, we investigate ocean heat budgets to determine the processes that lead to the unique pattern of deep, midlatitude heat storage in the Southern Ocean. In particular, we seek to understand the processes that transport the heat anomaly northward from the surface uptake region between 50° and 60°S and converge it in the upper ~1.5 km at 40°–45°S.

4. Relative roles of mean and eddy heat transports and convergences

a. Heat budget terms

Away from the surface, the ocean heat budget in a grid cell is given by

$$\rho_o c_p^0 dA\left[\frac{\partial(\theta dz)}{\partial t} = -\nabla_H \cdot (\mathbf{u}_H\theta + \mathbf{F}_{\text{subgrid}})dz - \delta_k(w\theta + F^z_{\text{subgrid}})\right], \quad (2)$$

where $\rho_o = 1035\,\text{kg m}^{-3}$ is the constant Boussinesq reference density, $c_p^0 = 3992\,\text{J kg}^{-1}\,\text{K}^{-1}$ is specific heat capacity, dA is the horizontal grid cell area, θ is potential temperature, ∇_H is the horizontal gradient operator, $\mathbf{u}_H$ is the horizontal velocity, $\mathbf{F}_{\text{subgrid}}$ represents the horizontal parameterized subgridscale temperature fluxes, δ_k is the discrete vertical difference operator, and w is vertical velocity. The term on the left-hand side of Eq. (2) is the heat content tendency, which is balanced by the

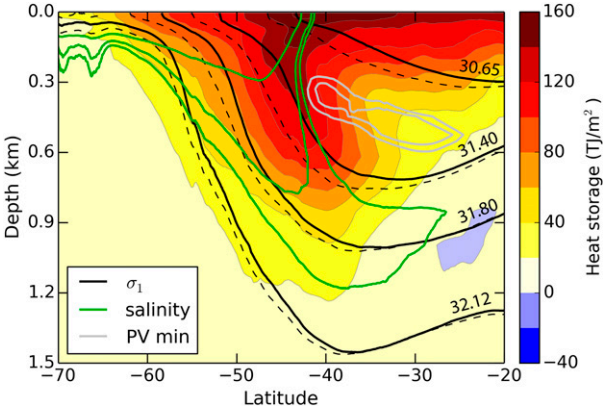

FIG. 4. Location of the heat content anomaly relative to Southern Ocean water masses. Background color shows the zonally integrated ocean heat gain at the time of CO_2 doubling, reproduced from Fig. 3b. Zonal average properties in the control simulation are overlaid as follows: isopycnals σ_1 in solid black with values shown on the far right (anomaly from 1000 kg m^{-3}), salinity contours in green (showing the freshwater tongue and indicating intermediate water), and planetary geostrophic potential vorticity (PV = $f\partial_z\sigma_0$) contours in gray (showing the PV minimum and indicating mode water). Isopycnals in the climate change simulation are shown in dashed black lines, with general deepening of the isopycnals associated with the heat uptake.

Unauthenticated | Downloaded 04/30/25 11:23 AM UTC

terms on the right-hand side: heat convergence due to the resolved advection and heat convergence due to parameterized subgrid-scale fluxes. The subgrid-scale fluxes included in the model are submesoscale restratification and vertical mixing (including turbulent diffusion, convection, and nonlocal KPP in the surface boundary layer). The model does not employ any mesoscale eddy parameterizations (either advective or diffusive) so that the entire mesoscale eddy contribution is contained in the resolved net advective convergence term.

To separately assess the contributions from the time mean circulation (i.e., the Eulerian mean) and mesoscale eddies, we perform an eddy-mean decomposition on the advective temperature flux $\overline{\mathbf{u}\theta}$. The eddy temperature flux is calculated as

$$\overline{\mathbf{u}'\theta'} = \overline{\mathbf{u}\theta} - \overline{\mathbf{u}}\,\overline{\theta}, \tag{3}$$

where the overbar indicates a long-term time average, and the prime is the deviation of 5-day averaged quantities from the longer time average. We follow the method in appendix B of Griffies et al. (2015), utilizing 20-yr monthly climatologies for the time averaging, which removes the influence of the seasonal cycle on the eddy calculation. The eddy heat convergence term will still contain contributions from interannual variability and correlated long-term trends in $\mathbf{u}$ and θ. However, comparison of convergences calculated over different time periods indicates that these contributions to the eddy convergence are minor.

It is worth noting that the resolved eddy heat flux, as calculated in Eq. (3), explicitly represents both isopycnal diffusion, arising from the action of resolved eddy stirring and mixing along-isopycnal temperature gradients, and what is usually thought of as eddy-induced advection in coarse-resolution models [i.e., as represented by the Gent and McWilliams (1990) parameterization (GM)]. As discussed in Kuhlbrodt et al. (2015), previous studies have not used the term "eddy advection" of heat consistently, which makes comparison between them difficult and confusing. Studies analyzing eddying models with no parameterized isopycnal diffusion (e.g., Wolfe et al. 2008; Morrison et al. 2013; Griffies et al. 2015), have used the terminology "eddy advection" to refer to the net resolved eddy heat flux, which is the sum of isopycnal diffusion and eddy-induced advection in coarse-resolution models. It is not a straightforward task to separate out the diffusive-like eddy flux from the net effect of the resolved mesoscale field, as calculated using the usual eddy-mean decomposition [i.e., Eq. (3)]. In contrast, studies using eddy-permitting models that utilize a parameterization for isopycnal diffusion, but not for eddy-induced advection (e.g., Exarchou et al. 2015; Kuhlbrodt et al. 2015), use the term "eddy advection" to refer to what they consider to be only the purely advective eddy flux (though this likely contains a small component of partially resolved diffusive-like effects also). Therefore an accurate comparison between the two types of studies should contrast the "eddy advection" from the former (Wolfe et al. 2008; Morrison et al. 2013; Griffies et al. 2015), with the sum of the "eddy advection" and parameterized isopycnal diffusion in the latter (Exarchou et al. 2015; Kuhlbrodt et al. 2015). In this study, in order to facilitate easier and more transparent comparison with coarse-resolution models and those using parameterized isopycnal diffusion, we choose to use the term "eddy advection and diffusion" or "net eddy flux" to refer to the net resolved eddy heat flux. This is equivalent to the "eddy advection" in Morrison et al. (2013) and Griffies et al. (2015).

The heat budget terms are calculated at each time step online [except the net eddy term, which is calculated as per Eq. (3) using 5-day averaged output] and averaged over the final 20 yr of the simulations.

b. *Vertical heat budget*

We integrate Eq. (2) over the region 30°–60°S for each vertical model level in the control simulation, showing the result in Fig. 5a, normalized by layer thickness. The values represent the net convergence at each depth, including both vertical fluxes and meridional fluxes across the boundaries at 30°S and 60°S. For the control simulation, the primary balance beneath the level of the deep Southern Ocean mixed layers (~500 m) is between heating by the time mean advection (blue) and cooling by the resolved eddies (green), consistent with previous studies (e.g., Gregory 2000; Wolfe et al. 2008), as explained in section 1. Convergence due to the submesoscale parameterization (magenta) and vertical mixing (black) are only significant within the mixed layer. Because of the short time scale of the simulation (200 yr), there remains a drift in the ocean heat content, shown by the tendency term (red). This drift in the control simulation is, on average, 27% of the climate change anomaly over the depth range 486–1075 m. Clearly the drift is not ideal and may influence our results. However, given that we find a strong dependence of the heat uptake on the mean state of the ocean, it is perhaps more important to minimize the bias in the circulation and tracer gradients in the control simulation compared with observations. The control simulation is initialized from observations such that the ocean tracer distributions and circulation drift farther away from the observed state the longer the simulation is run. Griffies et al. (2015) show that the rich eddy field in CM2.6

Unauthenticated | Downloaded 04/30/25 11:23 AM UTC

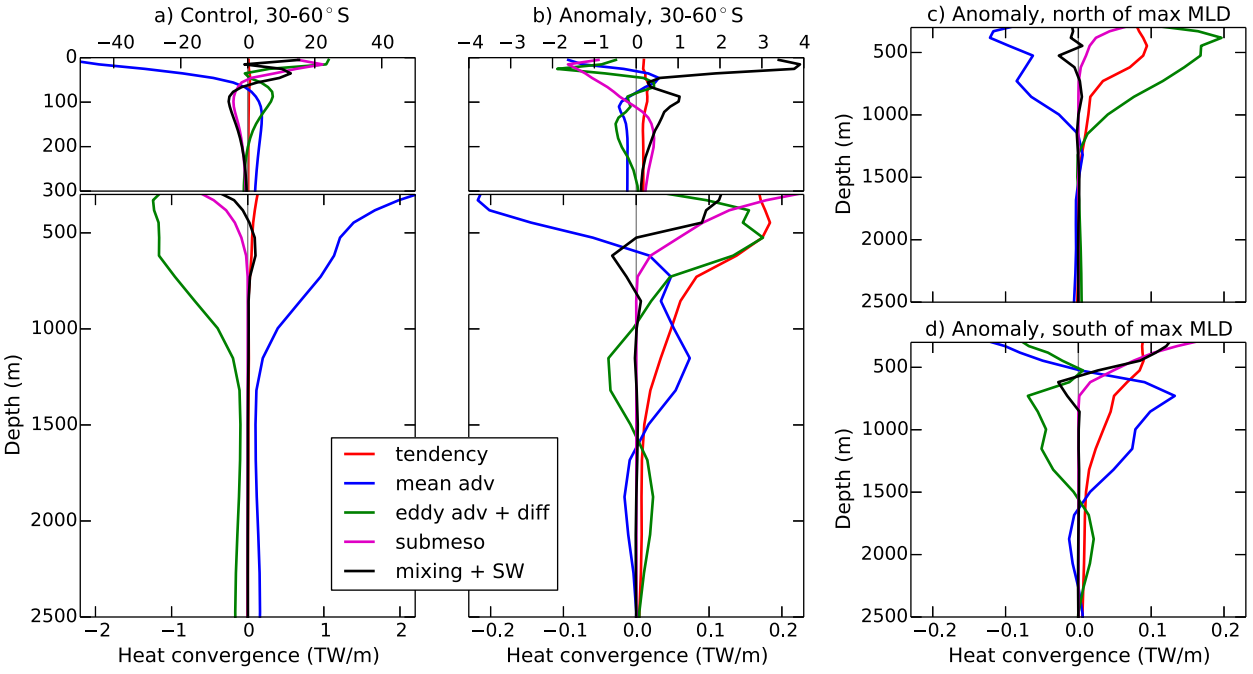

FIG. 5. Heat budget terms integrated horizontally and over years 61–80 (centered on CO_2 doubling), shown as heat convergence per unit depth. Positive values indicate warming processes. The rate of change of heat content (tendency), shown in red, is balanced by the sum of the mean advection (blue), the net resolved eddy contribution (green, including both advective and diffusive components), the submesoscale parameterization (magenta), and the net mixing (vertical diffusion and nonlocal KPP) combined with shortwave penetration (black). Depths below 2500 m are not shown because the terms are small and heat gain is insignificant. (a) Control simulation, integrated between 30° and 60°S. (b) Anomaly (1% yr^{-1} CO_2 experiment minus control), integrated between 30° and 60°S. The anomaly budget beneath 300-m depth and integrated over 30°–60°S [i.e., lower graph of (b)] is split into contributions from (c) north and (d) south of the deep mixed layers, as defined by the cyan line shown in Fig. 3a.

greatly reduces the ocean temperature bias compared with lower-resolution models.

The heat budget anomaly (1% yr^{-1} CO_2 simulation minus control) is shown in Fig. 5b. On first inspection, the response appears rather complicated, with different processes converging heat at different depths, leading to the positive tendency (red). Above 300 m, mixed layer processes [submesoscale restratification (magenta) and vertical mixing (black)] dominate the heat convergence. As it is expected that the heat content signal will spread to the base of the mixed layer, it is a more interesting problem to focus on the processes below this depth. As outlined in section 1, the two previously identified mechanisms that may drive deep Southern Ocean warming are: 1) an enhancement of the downward time mean advective heat transport or 2) a reduction in the upward net eddy heat transport (Fig. 1). In CM2.6, we find that both of these mechanisms are present, but their respective dominance alternates at different depths in the water column. Between 400- and 750-m depth, where the warming trend is maximum below the mixed layer, warming is primarily driven by a reduction in the net eddy cooling (green), consistent with a decrease in the along-isopycnal temperature gradient suggested by Gregory (2000). Beneath this, down to 1600 m, the warming is driven instead by an increased heat convergence by the time mean circulation (blue). Below 1600 m, the change in the net eddy heat flux again dominates. However, we note that there is very little heat content increase below 1600 m by the end of the simulation (Fig. 3b).

We find that more sense can be made of the complicated depth structure by considering the 30°–60°S heat budget anomaly below 300 m (i.e., the lower panel of Fig. 5b) split into a northern and southern region. We divide the region into two parts based on the location of the annual maximum mixed layer depth (shown by the cyan line in Fig. 3a), which is approximately spatially aligned with the heat content anomaly. This lateral division reveals that north of the deep mixed layers, the warming is driven primarily by a reduction in net eddy cooling (cf. green lines in Figs. 5a,c), whereas, south of the deep mixed layers, the warming is driven primarily by an enhancement of the time mean advection (blue line, Fig. 5d). This interesting distinction between the dominant heat budget

Unauthenticated | Downloaded 04/30/25 11:23 AM UTC

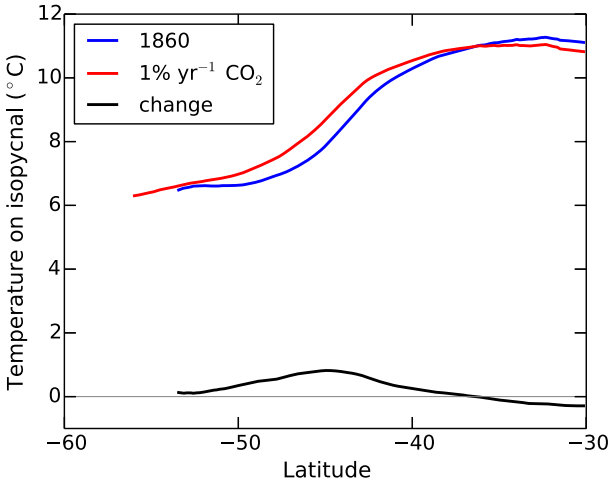

FIG. 6. Potential temperature on a representative middepth Southern Ocean isopycnal, in the control simulation (blue), the 1% yr^{-1} CO_2 experiment (red), and the difference (black), averaged over years 61–80. The isopycnal layer is bounded by the σ_1 anomalous density surfaces 30.65 and 31.40 kg m^{-3}, as labeled in Fig. 4. Data are only shown where the isopycnal thickness exceeds 50 m.

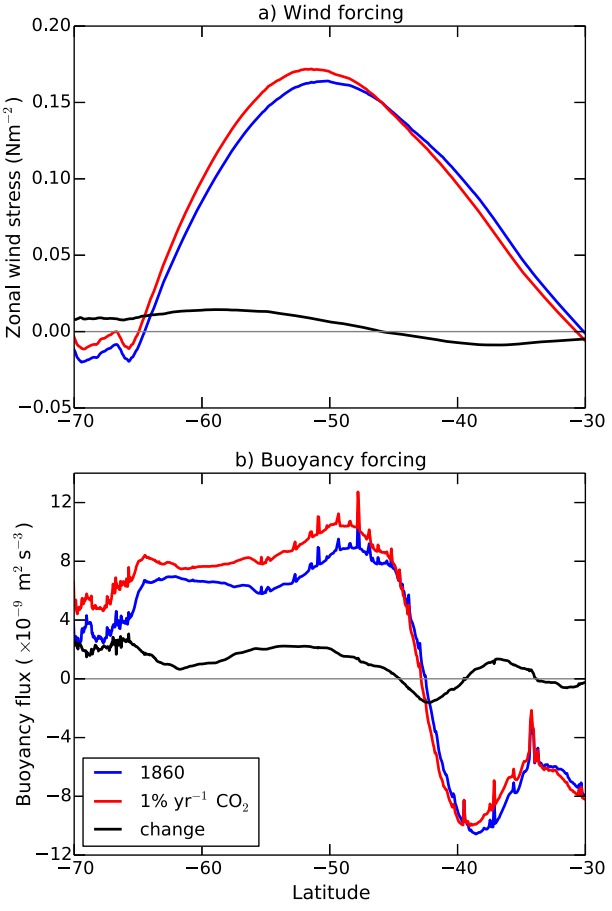

FIG. 7. Zonally averaged (a) zonal wind stress and (b) net surface buoyancy forcing acting on the ocean, including both heat and freshwater components. Positive buoyancy forcing decreases ocean density. The buoyancy forcing is computed using monthly averaged data according to $B = g/\rho_o[\alpha/c_p^0 Q + \beta S(\mathrm{FW})]$, where α is the thermal expansion coefficient, Q is the net heat flux, β is the haline contraction coefficient, S is sea surface salinity, and FW is the net freshwater flux. Colors show the forcing in the control simulation (blue), 1% yr^{-1} CO_2 experiment (red), and the difference between the two (black), all averaged over years 61–80. The spikes in the buoyancy forcing arise from river runoff into the ocean.

processes to the north and south of the deep mixed layers arises only when taking the difference between the 1% yr^{-1} CO_2 simulation and the control. In the control simulation, the heat budgets in the northern and southern regions of the Southern Ocean are qualitatively similar to that shown in Fig. 5a.

The lateral separation of these two distinct mechanisms (eddy vs mean) can be conceptually understood in terms of the climatological circulation and changes in isopycnal temperature gradients. The deep mixed layers, which we use to divide the northern and southern regions, are aligned with the location of mode water formation at roughly 40°–45°S. At these latitudes, the climatological meridional surface transport is convergent, which leads to subduction of the heat anomaly into the interior. The heat anomaly remains relatively fixed at the location of the deep mixed layers, rather than being further advected northward along the mode water pathways (Fig. 4). The temperature along a Southern Ocean isopycnal increases northward and downward away from the surface (Fig. 6). The meridional isopycnal temperature gradient decreases most rapidly just on the northern side of the peak warming anomaly (i.e., between ~35° and 45°S). The large reduction in net eddy cooling (i.e., a positive anomaly) north of the deep mixed layers (Fig. 5c) is consistent with the decrease in isopycnal temperature gradients there.

South of the deep mixed layers, between 500- and 1600-m depth, the increase in the time mean heat convergence, which is partially opposed by a corresponding increase in the net eddy heat divergence (Fig. 5d), is consistent with existing understanding of how mean and eddy volume transports respond to enhanced wind stress (e.g., Morrison and Hogg 2013). As the zonal wind stress and surface buoyancy forcing increase in the climate change simulation (Fig. 7), the upwelling limb of the residual overturning circulation increases. Warming at depth occurs because the increase in the downward time mean heat advection (blue) is larger than the increase in the upward net eddy heat flux (green). The increase in the mean advection is limited to the south of the deep mixed layers (cf. Figs. 5c,d), where the increasing wind stress drives enhanced upwelling. To the north of the

Unauthenticated | Downloaded 04/30/25 11:23 AM UTC

deep mixed layers, the wind stress decreases, resulting in decreased mean heat convergence.

In summary, we find evidence for both mechanisms previously identified for deep Southern Ocean warming. South of the deep mixed layers, the heat convergence is driven primarily by enhanced mean flow (consistent with Cai et al. 2010; Marshall and Zanna 2014; Bryan et al. 2014; Exarchou et al. 2015; Kuhlbrodt et al. 2015). North of the deep mixed layers, a reduction in the upward net eddy heat flux drives the warming, at least partially driven by decreasing isopycnal temperature gradients (as found by Gregory 2000; Dalan et al. 2005; Morrison et al. 2013). The spatial separation of warming mechanisms (mean flow in the south, eddies in the north), highlights the sensitivity of the results to the choice of averaging region and may explain the seemingly inconsistent results of previous studies regarding the dominant mechanisms.

c. Calculation of eddy heat diffusion

To determine whether the warming by eddies north of the deep mixed layers is due to changes in the eddy advective or eddy diffusive fluxes, we use the method of Lee et al. (2007) to separate the net eddy heat transport into diffusive and advective components. The net resolved meridional heat transport on an isopycnal layer can be written as

$$\rho_o c_p^0 \left[\overline{v\theta h} = \frac{\overline{vh}}{\overline{h}} \frac{\overline{\theta h}}{\overline{h}} \overline{h} + \overline{\left(v - \frac{\overline{vh}}{\overline{h}} \right) \left(\theta - \frac{\overline{\theta h}}{\overline{h}} \right) h} \right], \qquad (4)$$

where h is isopycnal thickness and v and θ are the meridional velocity and potential temperature on the isopycnal. The first term on the right-hand side is the advective heat transport due to the residual circulation $\overline{vh}$ (i.e., mean plus eddy advection), and the second term is the resolved eddy diffusion, arising because of correlations between deviations of v and θ on isopycnals. To calculate the net advective heat transport [first term on the right-hand side of Eq. (4)], we bin 5-day averages of v and θ onto 48 σ_1 density layers. We define isopycnals using σ_1, because nearly all of the heat transport anomaly is concentrated in the upper 2 km of the water column, and a comparison using σ_2 layers revealed insignificant differences. The depth integral of the eddy diffusion term [last term in Eq. (4)] is calculated as the residual between the depth-integrated net heat transport (i.e., the term on the left-hand side, calculated online on depth levels) and the net advective heat transport integrated over all isopycnals [first term on the right-hand side of Eq. (4)]. Unfortunately we are only able to calculate the depth-integrated eddy diffusion because of a lack of necessary online diagnostics to compute the net heat advection on individual isopycnal layers. Therefore, we only show the depth-integrated separation of the net eddy heat transport.

d. Meridional heat budget

Figure 8a shows the meridional heat budget for the control simulation. The meridional budget is calculated from Eq. (2), by taking the zonal and depth integral, as well as the cumulative integral from the south. We use a zonal average rather than a streamline average, even though the heat uptake features are not strictly zonal because closed circumpolar streamlines exist only for a small subset of the latitude range in which we are interested. Integrating Eq. (2) results in the tendency term (i.e., drift; red) and net resolved northward heat transport (green). The meridional parameterized submesoscale heat flux is orders of magnitude smaller than the resolved transport and is not shown. The heat content tendency and net northward transport are balanced by the cumulative integral from the south of the air–sea heat flux (black). The depth-integrated net heat transport (green) in the control is southward everywhere in the Southern Ocean. Over the latitude range 43°–56°S, the net heat transport is divergent (i.e., meridional heat transport $\partial_y > 0$), implying heat gain at the surface (given small heat content tendency). Elsewhere over the Southern Ocean, the ocean heat transport is convergent, and the modeled air–sea heat flux on average cools the ocean. The net resolved northward heat transport (green) is separated using the decompositions in Eqs. (3) and (4) into three components: the time mean advective heat transport (blue, equivalent to the blue lines in Fig. 5), the eddy advective heat transport (magenta), and the eddy diffusive heat transport (cyan). The magnitude and latitudinal shape of the eddy advective and diffusive transports are similar to those calculated using the 1/12° Ocean Circulation and Climate Advanced Model (OCCAM) by Lee et al. (2007). Both components of the net eddy heat transport are predominantly southward in the control simulation, representing a flattening of isopycnals by the eddy advective transport and downgradient temperature diffusion along isopycnals by the eddy diffusive transport.

The meridional heat budget anomaly under increasing CO_2 (Fig. 8b) is of interest because the northward transport of the heat anomaly by the ocean plays an important role in keeping SST low in the south and allowing for continued heat uptake by the Southern Ocean. The surface heat flux anomaly (black) into the ocean occurs primarily between 50° and 60°S (as shown previously in Fig. 2a). Heat storage (red) over this latitude range is small, and instead there is a large northward heat transport anomaly, increasing up to 45°S

Unauthenticated | Downloaded 04/30/25 11:23 AM UTC

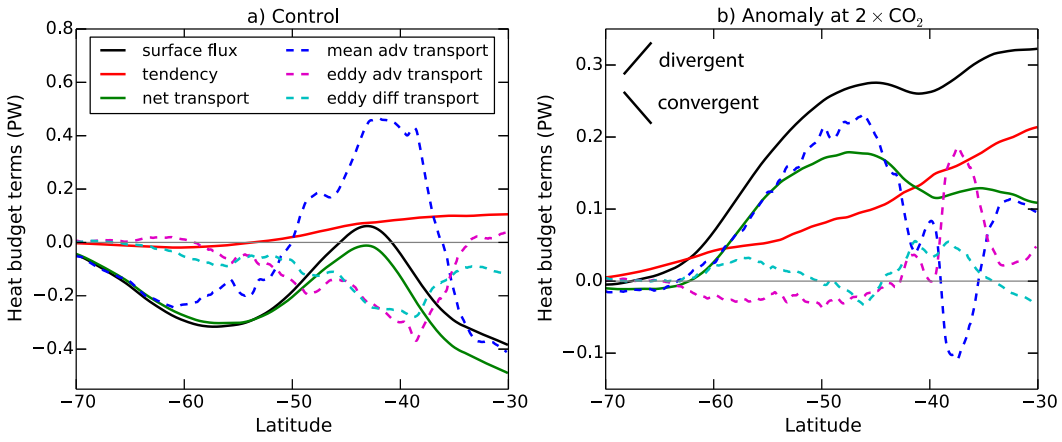

FIG. 8. Depth and zonally integrated meridional heat budget components for (a) the control simulation and (b) the anomaly from the control in the 1% yr^{-1} CO_2 experiment. The surface heat flux (black) and ocean heat content tendency (red) are shown as cumulative integrals computed northward from Antarctica. Positive surface heat flux indicates ocean heat gain. Combined with the surface heat flux and tendency, the net northward heat transport (green) closes the meridional ocean heat budget. The three dashed lines show the mean and eddy (further separated into advective and diffusive) components of the net northward heat transport. All terms are calculated as averages over years 61–80. The lines in the top left of (b) provide a guide for the reader as to where the transport components are divergent (positive slope) or convergent (negative slope).

(green), driven by the time mean advection (blue). We explore further in section 5 whether this enhancement of the northward heat transport by the time mean advection is due primarily to wind-driven increases in the Ekman transport or simply passive heat advection by the existing circulation. There is a strong convergence in the net heat transport (green) at ~40°–45°S, aligning with the peak warming signal seen in Figs. 3 and 4. The convergence is due to changes in the time mean heat advection (blue), partially opposed by changes in the eddy advection (magenta). While there is large northward increase in the mean advective heat transport between 45° and 50°S (blue), this drops off sharply to no change or even a southward anomaly between 35° and 45°S. This result—that the peak Southern Ocean heat convergence is driven primarily by enhanced mean flow, rather than eddies—is in agreement with the vertical heat budget south of the deep mixed layers (Fig. 5d) and those previous studies identifying this mechanism (Cai et al. 2010; Marshall and Zanna 2014; Bryan et al. 2014; Exarchou et al. 2015; Kuhlbrodt et al. 2015).

There are several possible drivers for the sharp decrease in the northward mean heat transport anomaly at 35°–45°S, including 1) decreased winds (Fig. 7a) resulting in less northward Ekman transport at this latitude range, 2) a southward shift of the subtropical gyre leading to a reorganization of the existing temperature distribution (e.g., Cai et al. 2010; Winton et al. 2013), or 3) a lightening of surface waters leading to reduced midlatitude convection and northward volume transport into the mode waters. We do not explore these possible mechanisms further in this paper, as further perturbation experiments would be required to distinguish between them.

While we find that changes in the eddy heat transport do not play a role in driving the prominent midlatitude heat convergence, eddies are very important for transporting the heat content anomaly farther north beyond the deep mixed layers. Between 34° and 44°S, a reduced southward transport (i.e., positive northward anomaly) by both the eddy advective and diffusive heat transports is responsible for four-fifths (78%) of the average northward heat transport anomaly at these latitudes (sum of cyan and magenta lines in Fig. 8b). The reader may find it useful to refer to the summary schematic in Fig. 11, which places the eddy heat transport change in the wider Southern Ocean context. The southward eddy diffusion decreases most strongly between 36° and 43°S (cyan line in Fig. 8b), consistent with where we expect the isopycnal temperature gradient to decrease the most (i.e., just to the north of the peak warming). Less southward eddy heat diffusion along isopycnals leads to a northward heat transport anomaly and a retaining of heat at depth. There is also a very strong decrease in the southward advective eddy heat transport (magenta) at 34°–40°S, though this is largely compensated by opposing changes in the mean heat transport (blue). We explore the drivers of these eddy heat transport changes in the next section. On the northern edge of the large positive eddy heat transport anomalies (i.e., 30°–38°S), the changes in the eddy terms are convergent. Therefore, the Southern Ocean warming north of 38°S is driven by changing eddy heat fluxes.

Unauthenticated | Downloaded 04/30/25 11:23 AM UTC

The structure of the mean and net eddy heat transport anomalies are similar to those found by Bryan et al. (2014). In a high-resolution CCSM 1% yr^{-1} increasing CO_2 simulation, they also found a large northward anomaly in the mean heat transport centered at 50°S and a large northward anomaly in the net eddy heat transport centered at 40°S.

e. *Drivers of changing eddy heat transport*

Given the importance of eddies for transporting heat northward from the peak convergence at 40°–45°S, we investigate further some of the drivers of the eddy heat transport changes: eddy kinetic energy, isopycnal temperature gradients, and isopycnal slopes (Fig. 9). Eddy kinetic energy (EKE) is calculated as $(\overline{u'^2} + \overline{v'^2})/2$, with primed quantities representing differences between 5-day averages and a 20-yr time mean, and averaged over the top 1590 m. The along-isopycnal temperature gradients and isopycnal slopes are averaged over the isopycnals bounded by the upper and lower σ_1 density surfaces (black lines) shown in Fig. 4, aligned with the main warming region and corresponding to roughly 0–1500 m. The along-isopycnal temperature gradients and isopycnal slopes were calculated by binning 5-day averaged data onto 21 σ_1 density surfaces between the two bounding isopycnals. Results in Figs. 9b,c were smoothed using a 5° meridional window and are shown only for latitudes where the total thickness of the included isopycnals is >300 m.

We wish to understand why there is a large reduction in both the diffusive and advective components of the southward eddy heat transport, resulting in the onward transport of the heat anomaly northward from the peak convergence region. Possible mechanisms for a reduction in the diffusive eddy heat transport could be either a decrease in eddy kinetic energy [according to the scaling of Ferrari and Nikurashin (2010)] or a decrease in the along-isopycnal meridional temperature gradient (Gregory 2000). We find that both of these mechanisms play a role in the CM2.6 climate change experiment. As seen in Fig. 8b, the southward eddy heat diffusion reduces most strongly between 36° and 43°S. The EKE decreases in the northern part of this range (35°–40°S; Fig. 9a) because of increased stratification (Fig. 9c) and decreased wind stress (Fig. 7a). The along-isopycnal temperature gradient decreases over a wider range, from ~33° to 45°S (Fig. 9b). While the absolute change in the isopycnal temperature gradient peaks at 42°S, the largest relative change occurs to the north of 41°S, where there is nearly uniform 30% decrease between ~33° and 41°S. Therefore, the reduction in the southward eddy heat diffusion is primarily due to a reduced isopycnal temperature gradient in the south and

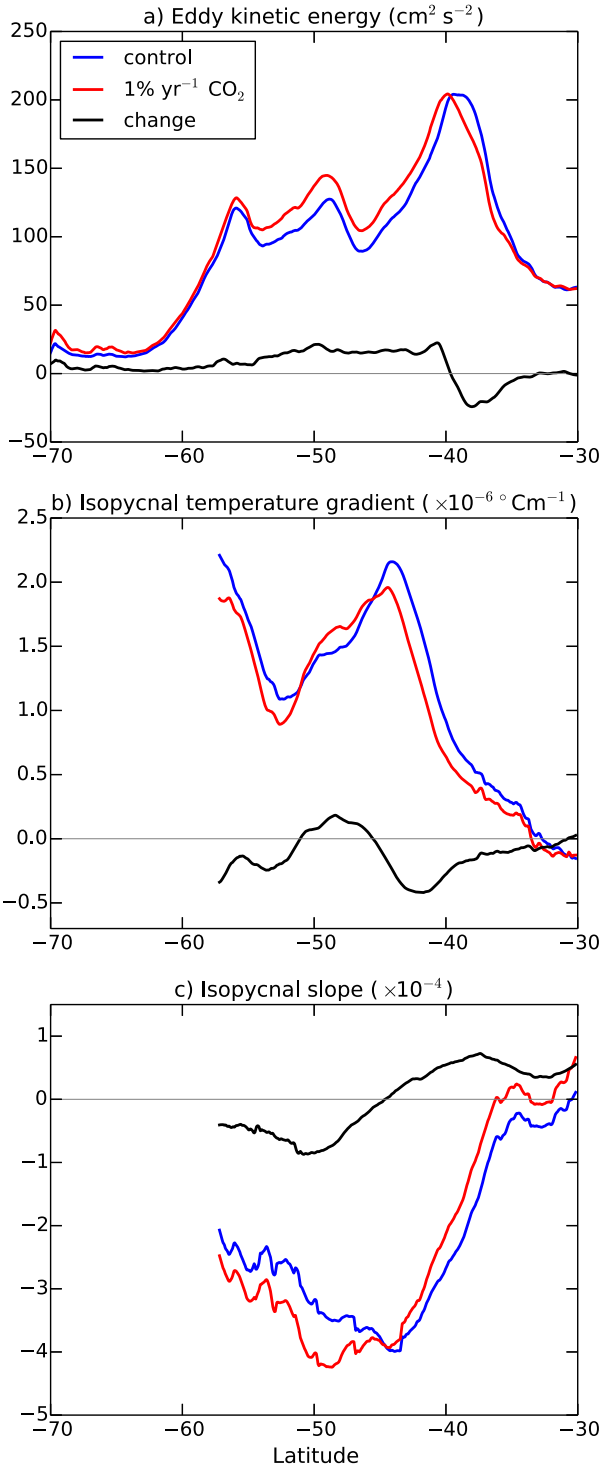

FIG. 9. Latitudinal distribution and response of zonally averaged eddy and isopycnal properties that impact the advective and diffusive eddy heat transports. (a) Eddy kinetic energy averaged over the top 1590 m. (b) The along-isopycnal temperature gradient, averaged over the isopycnals bounded by the upper and lower density surfaces (black lines) shown in Fig. 4 (roughly 0–1500 m). (c) Isopycnal slope, averaged over the same isopycnals as in (b). In (b) and (c), values are shown only for latitudes where the total thickness of the included isopycnals is >300 m. Meridional smoothing using a 5° window was applied in (b) and (c). All terms are calculated as averages over years 61–80.

Unauthenticated | Downloaded 04/30/25 11:23 AM UTC

both reduced EKE and isopycnal temperature gradient in the north. The sharp decrease in the southward eddy heat advection at 34°–40°S (Fig. 8b) is meridionally aligned with the decrease in EKE and corresponding flattening of isopycnal slopes (Figs. 9a,c). The downward movement of isopycnals (dashed black lines in Fig. 4) is enhanced in the region of maximum warming. The change in isopycnals is smaller outside this region because of the minimal water mass changes. Therefore isopycnal slopes flatten north of the peak warming and steepen south of the peak warming (Figs. 6, 9c).

In summary, a decrease in the southward eddy heat transport between 34° and 44°S is responsible for four-fifths of the northward heat transport anomaly over this latitude range (Fig. 11). The reason that eddies play such a significant role at this particular location—situated just to the north of the peak warming convergence—is because of the direct influence of the warming. The enhanced ocean heat content at 40°–45°S has the effect of flattening isopycnal slopes and decreasing eddy kinetic energy and along-isopycnal temperature gradients on the northern edge of the peak warming. These changes decrease the southward eddy heat transport. Significant decreases in both the advective and diffusive eddy heat transports allow for the northward transport of the heat content anomaly out of the Southern Ocean. Without the eddy transport changes, more heat would remain trapped in the Southern Ocean, leading to a larger increase in SST and less ocean heat uptake.

5. Impact of enhanced upwelling on heat uptake

In section 4, we saw that it is primarily an enhancement of the mean heat advection that transports the heat anomaly away from where it is taken up in the high latitudes, northward to the midlatitude deep mixed layers. As indicated by Eq. (1), the mean heat advection could increase via two possible mechanisms: either the rate of upwelling and velocity in the Ekman layer could increase and transport more surface water northward, or increased temperatures could lead to a passive advection of the heat content anomaly by the existing circulation. In this section we investigate this question by separating the influence of changing temperature and velocity on the net heat advection. To account for the role of eddies in Eq. (1), we apply an eddy-mean decomposition to the velocity and potential temperature:

$$\Delta\overline{v\theta} = \Delta\overline{(\overline{v}+v')(\overline{\theta}+\theta')} = \Delta(\overline{v}\,\overline{\theta}) + \Delta\overline{v'\theta'}. \qquad (5)$$

Then expressing the mean velocity in the climate change experiment as $\overline{v}_{CO_2} = \overline{v}_{1860} + \Delta\overline{v}$ (and similarly for

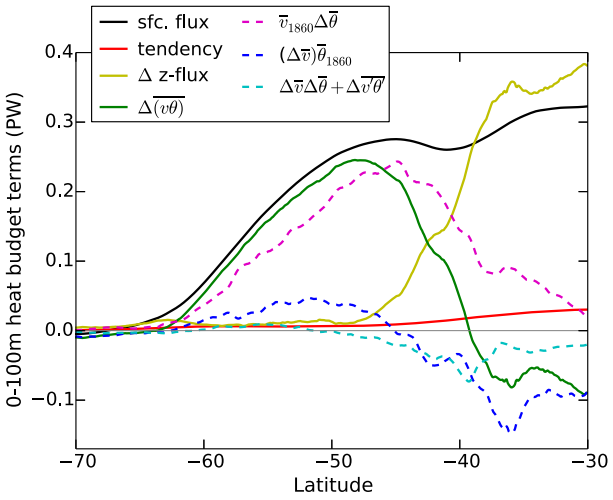

FIG. 10. Heat budget anomaly terms for the upper 0–100 m, integrated northward from Antarctica. The surface heat flux (black) is balanced by the ocean heat content tendency (red), net northward heat transport (green), and downward heat flux across 100-m depth (yellow). The three dashed lines are the components of the net northward heat transport anomaly (green). These components, from Eq. (6), are passive heat advection by the time mean preindustrial circulation (magenta), redistribution of the preindustrial ocean heat content (blue), and a component due to changes in both circulation and temperature, including eddies (cyan). All temperature transports have been converted to heat transports by a multiplication factor of $\rho_o c_p^0$ (not shown in legend).

potential temperature) leads to the following separation for the net temperature transport anomaly:

$$\Delta\overline{v\theta} = \overline{v}_{1860}\Delta\overline{\theta} + (\Delta\overline{v})\overline{\theta}_{1860} + (\Delta\overline{v}\Delta\overline{\theta} + \Delta\overline{v'\theta'}), \qquad (6)$$

where Δ indicates a difference between the 1% yr^{-1} CO_2 experiment and the control, and the 1860 subscript refers to quantities in the control simulation. Averages are taken over a 20-yr period, and eddy quantities are calculated using 5-day averaged data and by removing the seasonal cycle, as explained following Eq. (3). The first term on the right-hand side of Eq. (6) represents passive advection of the temperature anomaly by the existing time mean circulation in the control simulation. The second term represents a redistribution of the original temperature structure and could be important if there are significant changes in circulation. The final two terms represent altered temperature transport due to changes in both circulation and temperature, including eddy changes. Previous coarse-resolution model studies have generally considered these two terms to be small (e.g., Winton et al. 2013), and we find that south of the deep mixed layers, the net eddy change is small (sum of magenta and cyan lines in Fig. 8b).

The dashed lines in Fig. 10 represent the terms in Eq. (6) integrated zonally and over the top 100-m depth. We

Unauthenticated | Downloaded 04/30/25 11:23 AM UTC

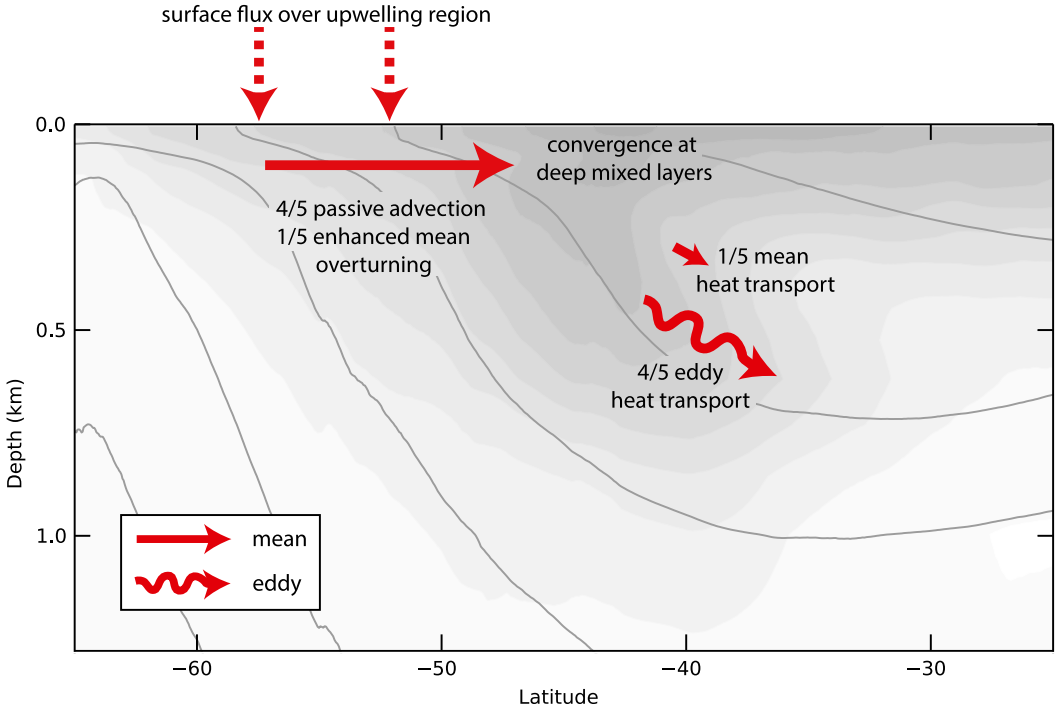

FIG. 11. Schematic illustrating the key mechanisms of the heat transport anomaly in CM2.6. Background shading shows ocean heat storage, and gray lines indicate isopycnals. Red arrows show anomalies of the air–sea flux (dashed), mean heat transport (solid), and eddy heat transport (squiggly). The region 50°–60°S dominates the global surface heat uptake, because upwelling keeps SST consistently cool, as the atmosphere above warms strongly. The heat is advected away from the uptake region primarily (four-fifths) by the existing time mean circulation, with a small contribution (one-fifth) from the enhanced overturning circulation. There is a strong heat convergence at the deep mixed layers (40°–45°S) because of the limited mean heat transport anomaly on the northern side. Instead, eddies account for four-fifths of the net heat transport anomaly on the northern edge of the main heat convergence.

find that it is only necessary to examine the upper 100 m, because this accounts for nearly all of the northward transport of the additional absorbed heat southward of ~47°S (cf. green and black lines). South of the deep mixed layers, there is only a minimal transfer of heat downward below 100 m (yellow line), with the vast majority remaining in the surface Ekman layer. We find that passive advection (magenta) is the dominant term, accounting for four-fifths (78%) of the surface northward heat transport anomaly south of the deep mixed layers (averaged between 48° and 58°S). The maximum strength of the modeled residual overturning (upper cell) in the Southern Ocean increases by 12% at the time of double CO_2 relative to the control simulation, driven by both increased wind stress and surface buoyancy forcing (Fig. 7). The enhanced overturning leads to a nonnegligible redistribution term (blue), which accounts for 20% of the northward heat transport anomaly south of the deep mixed layers. These results are summarized in Fig. 11 and are qualitatively consistent with Marshall et al. (2015), who also found that passive advection of the heat content anomaly dominates.

While increased upwelling has a relatively minor impact in this study relative to the passive advection term, the fact that it is still a significant fraction (20%) of the heat transport anomaly indicates that overturning circulation change could be a dominant mechanism controlling Southern Ocean heat uptake in models with larger wind stress changes and more responsive ocean circulation. In the eddying CM2.6 simulation presented here, the maximum wind stress increases by 5%, and the surface buoyancy forcing, averaged between 50° and 60°S, increases by 28% at the time of doubled CO_2 (Fig. 7). As a result of these atmospheric forcing changes, the Southern Ocean residual overturning increases by 12% in the climate change experiment. Given the coupled nature of the model, it is not possible to separate out the overturning sensitivity to the wind and buoyancy forcing changes or the degree of eddy compensation. However, results from idealized modeling studies would suggest that the 12% increase in overturning is driven primarily by the enhanced surface buoyancy forcing (Morrison et al. 2011), or at least by wind-induced feedbacks in the buoyancy forcing

Unauthenticated | Downloaded 04/30/25 11:23 AM UTC

(Abernathey et al. 2011). The relatively small wind stress response and the expected eddy compensation (e.g., Hallberg and Gnanadesikan 2006; Morrison and Hogg 2013) lead us to hypothesize that the direct effect of the enhanced wind stress via the Ekman transport plays a very minor role in the residual overturning transport change in CM2.6. However, as we discuss in the following section, overturning change may play a larger role in driving Southern Ocean heat uptake and northward transport in the real ocean and other models.

6. Discussion and conclusions

Recent observations and model simulations have noted the dominant role of the Southern Ocean in global oceanic heat uptake. Sustained heat uptake over the Southern Ocean occurs because the northward transport of the heat content anomaly combined with cold upwelling keeps SST cool in the uptake region, even as the atmosphere warms. In this paper, we have used an eddying global climate model to investigate the processes that transport the heat anomaly northward and downward from the surface uptake region (50°–60°S) and converge it at middepths in the midlatitude Southern Ocean (40°–45°S).

Previous studies disagree on whether the heat transport anomaly and warming are driven primarily by changes in the time mean or eddy heat transport (Fig. 1). We find that changes in both the mean flow and eddies are dynamically significant. However, there is a geographical separation of the two mechanisms, as shown in the summary schematic (Fig. 11). South of the deep mixed layers, a large northward increase in the mean advective heat transport in the surface Ekman layer moves the heat content anomaly away from the uptake region. The northward increase in the mean heat transport stops abruptly at the deep mixed layers, with only minimal advection into the mode water pathways, thereby resulting in the large midlatitude heat convergence. The reason for the discontinuity in the mean heat transport anomaly at the deep mixed layers remains an interesting open question for future studies.

The intense warming at the deep mixed layers alters the isopycnal slopes and along-isopycnal temperature gradients on the northern edge of the peak warming and thus drives a decrease in southward eddy heat fluxes there (i.e., a northward anomaly). Between 34° and 44°S, eddies account for four-fifths (78%) of the anthropogenic northward heat transport. Without these eddy transport changes, more heat would remain trapped in the Southern Ocean, leading to a larger increase in SST and less ocean heat uptake. Because different mechanisms dominate in different parts of the Southern Ocean, budget integrals are highly sensitive to the choice of averaging region. This may explain the seemingly inconsistent results of previous studies regarding the dominant mechanisms.

In this study, enhanced Southern Ocean upwelling plays a small but nonnegligible role in the northward heat transport anomaly south of the deep mixed layers. In CM2.6, the upper residual overturning increases by 12%, predominantly driven by enhanced surface buoyancy forcing. This 12% increase in upwelling accounts for 20% of the northward heat transport anomaly. While the upwelling increase has a relatively minor impact on the heat transport compared with the passive advection component in the model, larger wind stress changes in the real world would indicate that enhanced upwelling could be important for driving the observed ocean heat uptake. The 1% yr^{-1} CO_2 simulation analyzed here has a small wind stress change (+5% after 70 yr) because of the lack of ozone forcing, as well as CM2.6 likely suffering from a common model bias for grossly underestimating wind stress changes (e.g., Swart and Fyfe 2012). Historical reanalysis products indicate that Southern Ocean wind stress may have increased by ~15% from 1979 to 2010 (Swart and Fyfe 2012). A larger wind stress increase would drive stronger upwelling and therefore lead to a larger role for ocean circulation change in Southern Ocean heat uptake and transport.

Coarse-resolution models generally have a more responsive overturning circulation than eddying models as a result of inadequate eddy parameterizations (e.g., Hallberg and Gnanadesikan 2006; Morrison et al. 2013). Our results imply that if coarse-resolution models overestimate the overturning response to enhanced wind stress, they will simulate a larger northward heat transport anomaly and therefore a larger simulated Southern Ocean heat uptake.

The results of this study give insight into some of the mechanisms that may explain the huge range of Southern Ocean heat uptake in the CMIP5 model suite. The parameterization of eddies in these models may be expected to play a critical role in controlling the rate of anthropogenic heat transport out of the Southern Ocean, and thus also in setting the magnitude of heat uptake. Bryan et al. (2014) show that a coarse-resolution model with a variable GM coefficient is able to produce approximately the same pattern of eddy heat transport change, but of reduced magnitude compared with a higher-resolution model. Furthermore, models with more sensitive overturning circulation, or larger wind stress changes, may be expected to have increased heat uptake compared to those with little overturning change.

Unauthenticated | Downloaded 04/30/25 11:23 AM UTC

While our study has provided insight into the role of eddies and the overturning circulation in Southern Ocean heat uptake, our understanding remains far from complete. We have not considered the impact of atmospheric processes, such as aerosols and clouds, that likely also affect the magnitude of heat uptake. It is also possible that processes that are insignificant in CM2.6, such as vertical diffusion, may play a more significant role in other model simulations.

Acknowledgments. We thank Carolina Dufour and Ivy Frenger for conversations that helped clarify ideas and analyses, as well as three anonymous reviewers for helpful and encouraging comments. AKM was supported by the U.S. Department of Energy under Contract DE-SC0012457. JLS acknowledges NSF's Southern Ocean Carbon and Climate Observations and Modeling project under Award PLR-1425989.

REFERENCES

Abernathey, R., J. Marshall, and D. Ferreira, 2011: The dependence of Southern Ocean meridional overturning on wind stress. *J. Phys. Oceanogr.*, **41**, 2261–2278, doi:10.1175/JPO-D-11-023.1.

Böning, C. W., A. Dispert, M. Visbeck, S. R. Rintoul, and F. U. Schwarzkopf, 2008: The response of the Antarctic Circumpolar Current to recent climate change. *Nat. Geosci.*, **1**, 864–869, doi:10.1038/ngeo362.

Bryan, F. O., P. R. Gent, and R. Tomas, 2014: Can Southern Ocean eddy effects be parameterized in climate models? *J. Climate*, **27**, 411–425, doi:10.1175/JCLI-D-12-00759.1.

Cai, W., T. Cowan, S. Godfrey, and S. Wijffels, 2010: Simulations of processes associated with the fast warming rate of the southern midlatitude ocean. *J. Climate*, **23**, 197–206, doi:10.1175/2009JCLI3081.1.

Dalan, F., P. H. Stone, and A. P. Sokolov, 2005: Sensitivity of the ocean's climate to diapycnal diffusivity in an EMIC. Part II: Global warming scenario. *J. Climate*, **18**, 2482–2496, doi:10.1175/JCLI3412.1.

Delworth, T. L., and Coauthors, 2012: Simulated climate and climate change in the GFDL CM2.5 high-resolution coupled climate model. *J. Climate*, **25**, 2755–2781, doi:10.1175/JCLI-D-11-00316.1.

Ducet, N., P. Y. Le Traon, and G. Reverdin, 2000: Global high-resolution mapping of ocean circulation from TOPEX/Poseidon and ERS-1 and -2. *J. Geophys. Res.*, **105**, 19 477–19 498, doi:10.1029/2000JC900063.

Dufour, C., and Coauthors, 2015: Role of mesoscale eddies in cross-frontal transport of heat and biogeochemical tracers in the Southern Ocean. *J. Phys. Oceanogr.*, **45**, 3057–3081, doi:10.1175/JPO-D-14-0240.1.

Durack, P. J., P. J. Gleckler, F. W. Landerer, and K. E. Taylor, 2014: Quantifying underestimates of long-term upper-ocean warming. *Nat. Climate Change*, **4**, 999–1005, doi:10.1038/nclimate2389.

Exarchou, E., T. Kuhlbrodt, J. M. Gregory, and R. S. Smith, 2015: Ocean heat uptake processes: A model intercomparison. *J. Climate*, **28**, 887–908, doi:10.1175/JCLI-D-14-00235.1.

Ferrari, R., and M. Nikurashin, 2010: Suppression of eddy diffusivity across jets in the Southern Ocean. *J. Phys. Oceanogr.*, **40**, 1501–1519, doi:10.1175/2010JPO4278.1.

Fox-Kemper, B., and Coauthors, 2011: Parameterization of mixed layer eddies. III: Implementation and impact in global ocean climate simulations. *Ocean Modell.*, **39**, 61–78, doi:10.1016/j.ocemod.2010.09.002.

Frölicher, T. L., J. L. Sarmiento, D. J. Paynter, J. P. Dunne, J. P. Krasting, and M. Winton, 2015: Dominance of the Southern Ocean in anthropogenic carbon and heat uptake in CMIP5 models. *J. Climate*, **28**, 862–886, doi:10.1175/JCLI-D-14-00117.1.

Gent, P. R., and J. C. McWilliams, 1990: Isopycnal mixing in ocean circulation models. *J. Phys. Oceanogr.*, **20**, 150–155, doi:10.1175/1520-0485(1990)020<0150:IMIOCM>2.0.CO;2.

Gille, S. T., 2002: Warming of the Southern Ocean since the 1950s. *Science*, **295**, 1275–1277, doi:10.1126/science.1065863.

Gregory, J. M., 2000: Vertical heat transports in the ocean and their effect on time-dependent climate change. *Climate Dyn.*, **16**, 501–515, doi:10.1007/s003820000059.

Griffies, S. M., 2012: Elements of the Modular Ocean Model (MOM): 2012 release. GFDL Ocean Group Tech. Rep. 7, 614 pp. [Available online at http://www.mom-ocean.org/web/docs/project/MOM5_elements.pdf.]

——, and R. W. Hallberg, 2000: Biharmonic friction with a Smagorinsky-like viscosity for use in large-scale eddy-permitting ocean models. *Mon. Wea. Rev.*, **128**, 2935–2946, doi:10.1175/1520-0493(2000)128<2935:BFWASL>2.0.CO;2.

——, and Coauthors, 2015: Impacts on ocean heat from transient mesoscale eddies in a hierarchy of climate models. *J. Climate*, **28**, 952–977, doi:10.1175/JCLI-D-14-00353.1.

Hallberg, R., 2013: Using a resolution function to regulate parameterizations of oceanic mesoscale eddy effects. *Ocean Modell.*, **72**, 92–103, doi:10.1016/j.ocemod.2013.08.007.

——, and A. Gnanadesikan, 2006: The role of eddies in determining the structure and response of the wind-driven Southern Hemisphere overturning: Results from the Modeling Eddies in the Southern Ocean (MESO) project. *J. Phys. Oceanogr.*, **36**, 2232–2252, doi:10.1175/JPO2980.1.

IPCC, 2013: *Climate Change 2013: The Physical Science Basis*. Cambridge University Press, 1535 pp., doi:10.1017/CBO9781107415324.

Kuhlbrodt, T., and J. M. Gregory, 2012: Ocean heat uptake and its consequences for the magnitude of sea level rise and climate change. *Geophys. Res. Lett.*, **39**, L18608, doi:10.1029/2012GL052952.

——, ——, and L. C. Shaffrey, 2015: A process-based analysis of ocean heat uptake in an AOGCM with an eddy-permitting ocean component. *Climate Dyn.*, **45**, 3205–3226, doi:10.1007/s00382-015-2534-0.

Large, W. G., J. C. McWilliams, and S. C. Doney, 1994: Oceanic vertical mixing: A review and a model with a nonlocal boundary layer parameterization. *Rev. Geophys.*, **32**, 363–403, doi:10.1029/94RG01872.

Lee, M.-M., A. J. G. Nurser, A. C. Coward, and B. A. de Cuevas, 2007: Eddy advective and diffusive transports of heat and salt in the Southern Ocean. *J. Phys. Oceanogr.*, **37**, 1376–1393, doi:10.1175/JPO3057.1.

Le Traon, P. Y., F. Nadal, and N. Ducet, 1998: An improved mapping method of multisatellite altimeter data. *J. Atmos. Oceanic Technol.*, **15**, 522–534, doi:10.1175/1520-0426(1998)015<0522:AIMMOM>2.0.CO;2.

Unauthenticated | Downloaded 04/30/25 11:23 AM UTC

Levitus, S., and Coauthors, 2012: World ocean heat content and thermosteric sea level change (0–2000 m), 1955–2010. *Geophys. Res. Lett.*, **39**, L10603, doi:10.1029/2012GL051106.

Marshall, D. P., and L. Zanna, 2014: A conceptual model of ocean heat uptake under climate change. *J. Climate*, **27**, 8444–8465, doi:10.1175/JCLI-D-13-00344.1.

Marshall, J., J. R. Scott, K. C. Armour, J. M. Campin, M. Kelley, and A. Romanou, 2015: The ocean's role in the transient response of climate to abrupt greenhouse gas forcing. *Climate Dyn.*, **44**, 2287–2299, doi:10.1007/s00382-014-2308-0.

Morrison, A. K., and A. McC. Hogg, 2013: On the relationship between Southern Ocean overturning and ACC transport. *J. Phys. Oceanogr.*, **43**, 140–148, doi:10.1175/JPO-D-12-057.1.

——, ——, and M. L. Ward, 2011: Sensitivity of the Southern Ocean overturning circulation to surface buoyancy forcing. *Geophys. Res. Lett.*, **38**, L14602, doi:10.1029/2011GL048031.

——, O. A. Saenko, A. McC. Hogg, and P. Spence, 2013: The role of vertical eddy flux in Southern Ocean heat uptake. *Geophys. Res. Lett.*, **40**, 5445–5450, doi:10.1002/2013GL057706.

——, T. L. Frölicher, and J. L. Sarmiento, 2015: Upwelling in the Southern Ocean. *Phys. Today*, **68**, 27–32, doi:10.1063/PT.3.2654.

Roemmich, D., J. Church, J. Gilson, D. Monselesan, P. Sutton, and S. Wijffels, 2015: Unabated planetary warming and the spatial structure of ocean warming since 2006. *Nat. Climate Change*, **5**, 240–245, doi:10.1038/nclimate2513.

Stouffer, R. J., J. Russell, and M. J. Spelman, 2006: Importance of oceanic heat uptake in transient climate change. *Geophys. Res. Lett.*, **33**, L17704, doi:10.1029/2006GL027242.

Swart, N. C., and J. C. Fyfe, 2012: Observed and simulated changes in the Southern Hemisphere surface westerly wind-stress. *Geophys. Res. Lett.*, **39**, L16711, doi:10.1029/2012GL052810.

Waugh, D. W., F. Primeau, T. Devries, and M. Holzer, 2013: Recent changes in the ventilation of the southern oceans. *Science*, **339**, 568–570, doi:10.1126/science.1225411.

Winton, M., S. M. Griffies, B. L. Samuels, J. L. Sarmiento, and T. L. Frölicher, 2013: Connecting changing ocean circulation with changing climate. *J. Climate*, **26**, 2268–2278, doi:10.1175/JCLI-D-12-00296.1.

Wolfe, C. L., P. Cessi, J. L. McClean, and M. E. Maltrud, 2008: Vertical heat transport in eddying ocean models. *Geophys. Res. Lett.*, **35**, L23605, doi:10.1029/2008GL036138.

Unauthenticated | Downloaded 04/30/25 11:23 AM UTC